

Pushing the limit of molecular dynamics with *ab initio* accuracy to 100 million atoms with machine learning

Weile Jia

jiaweile@berkeley.edu

University of California, Berkeley
Berkeley, California

Han Wang

wang_han@iapcm.ac.cn

Laboratory of Computational Physics,
Institute of Applied Physics and
Computational Mathematics
Beijing, China

Mohan Chen

mohanchen@pku.edu.cn

CAPT, HEDPS, College of
Engineering, Peking University
Beijing, China

Denghui Lu

denghui@pku.edu.cn

CAPT, HEDPS, College of
Engineering, Peking University
Beijing, China

Jiduan Liu

1700017857@pku.edu.cn

Peking University
Beijing, China

Lin Lin

linlin@math.berkeley.edu

University of California, Berkeley
Lawrence Berkeley National
Laboratory
Berkeley, California

Roberto Car

rcar@princeton.edu

Princeton University
Princeton, NJ

Weinan E

weinan@math.princeton.edu

Princeton University
Princeton, NJ

Linfeng Zhang*

linfengz@princeton.edu

Princeton University
Princeton, NJ

ABSTRACT

For 35 years, *ab initio* molecular dynamics (AIMD) has been the method of choice for understanding complex materials and molecules at the atomic scale from first principles. However, most applications of AIMD are limited to systems with thousands of atoms due to the high computational complexity. We report that a machine learning-based molecular simulation protocol (Deep Potential Molecular Dynamics), driven by a highly optimized code (GPU DeePMD-kit) on the Summit supercomputer, has greatly expanded the capabilities of MD simulation with *ab initio* accuracy, pushing its limit to simulation of over 100 million atoms for one nanosecond per day. Our code can efficiently scale up to the entire Summit supercomputer, reaching 86 PFLOPS in double precision (43% of the peak) and 137 PFLOPS in mixed precision. This success opens the door to the modeling of atomic processes in realistic materials and molecular systems with *ab initio* accuracy.

KEYWORDS

Deep potential molecular dynamics, *ab initio* molecular dynamics, machine learning, GPU, heterogeneous architecture, Summit

*Corresponding author

Permission to make digital or hard copies of all or part of this work for personal or classroom use is granted without fee provided that copies are not made or distributed for profit or commercial advantage and that copies bear this notice and the full citation on the first page. Copyrights for components of this work owned by others than ACM must be honored. Abstracting with credit is permitted. To copy otherwise, or republish, to post on servers or to redistribute to lists, requires prior specific permission and/or a fee. Request permissions from permissions@acm.org.

SC '20, November 17–22, 2020, Atlanta, GA, USA

© 2020 Association for Computing Machinery.

ACM ISBN 978-x-xxxx-xxxx-x/YY/MM...\$15.00

<https://doi.org/10.1145/nnnnnnnn.nnnnnnnn>

ACM Reference Format:

Weile Jia, Han Wang, Mohan Chen, Denghui Lu, Jiduan Liu, Lin Lin, Roberto Car, Weinan E, and Linfeng Zhang. 2020. Pushing the limit of molecular dynamics with *ab initio* accuracy to 100 million atoms with machine learning. In *The International Conference for High Performance Computing, Networking, Storage, and Analysis (SC '20)*, November 17–22, 2020, Atlanta, GA, USA. ACM, New York, NY, USA, 12 pages. <https://doi.org/10.1145/nnnnnnnn.nnnnnnnn>

1 JUSTIFICATION FOR PRIZE

Record molecular dynamics simulation of >100 million atoms with *ab initio* accuracy. For a 113-million-atom copper system, time-to-solution of 7.3×10^{-10} s/step/atom, or equivalently one nanosecond/day, >1000× improvement w.r.t state-of-the-art. Double precision performance of 86 PFLOPS on 4,560 nodes of Summit (43% of the peak); mixed precision of 137 PFLOPS.

2 PERFORMANCE ATTRIBUTES

Performance attribute	Our submission
Category of achievement	Time-to-solution, scalability
Type of method used	Deep potential molecular dynamics
Results report on basis of	Whole application including I/O
Precision reported	Double precision, mixed precision
System scale	Measured on full system
Measurements	Timers, FLOP count

3 OVERVIEW OF THE PROBLEM

3.1 *ab initio* molecular dynamics

Molecular dynamics (MD) [24, 56] is an *in silico* simulation tool for describing atomic processes that occur in materials and molecules. The accuracy of MD lies in the description of the atomic interactions,

for which the *ab initio* molecular dynamics (AIMD) scheme [13, 42] stands out by evolving atomic systems with the interatomic forces generated on-the-fly using first-principles methods such as the density functional theory (DFT) [34]. AIMD permits chemical bond cleavage and formation events to occur and accounts for electronic polarization effects. Due to the faithful description of atomic interactions by DFT, AIMD has been by far the major avenue for microscopic understandings of a broad spectrum of issues, such as drug discovery [5, 14], complex chemical processes [16, 36], and nanotechnology [47], etc..

The computational cost of AIMD generally scales cubically with respect to the number of electronic degrees of freedom. On a desktop workstation, the typical spatial and temporal scales achievable by AIMD are ~ 100 atoms and ~ 10 picoseconds. In the past thirteen years (2006 to 2019), the peak performance of the world’s fastest supercomputer has increased 550-folds, (from 360 TFLOPS of Blue-Gene/L to 200 PFLOPS of Summit), but the system size recorded has only increased by 8 times (from 1K Molybdenum atoms with 12K valence electrons [26] to 11K Magnesium atoms with 105K valence electrons [21]), which obeys almost perfectly the cubic-scaling law. Linear-scaling DFT methods [23, 44, 48, 62] have been under active development, yet the pre-factor in the complexity is still large, and the codes are not suitable for long-time MD simulation.

For problems in complex chemical reactions [37, 43], electrochemical cells [31], nanocrystalline materials [49, 50], irradiation damages [25], and dynamic fracture and crack propagation [57, 58], etc., the required system size typically ranges from thousands to hundreds of millions of atoms. Some of the problems demand an even higher accuracy, e.g., the so-called chemical accuracy (~ 1 kcal/mol), for which even DFT would fail and more expensive methods like the CCSD(T) [46], whose computational complexity scales with the seventh power of the system size, are required. Although there have been a host of empirical force field (EFF)-based MD schemes (see, e.g., Refs. [12, 29, 52, 61]), which can easily scale up to millions, or even trillions, of atoms, their accuracy is often in question. In particular, it has been challenging to develop EFFs for cases involving multiple elements or bond formation and cleavage, and for many practical problems there are no suitable EFFs available. Above all, there is an urgent demand in the MD community for fundamentally boosting the efficiency of AIMD while keeping its accuracy.

3.2 Deep Potential Molecular Dynamics

Recently, machine learning based MD (MLMD) schemes [9, 10, 18, 27, 51, 54, 66, 67] offered a new paradigm for boosting AIMD by means of ML-based models trained with *ab initio* data. The Deep Potential (DP) method has demonstrated to achieve an accuracy comparable to AIMD, and an efficiency close to EFF-based MD [66, 67]. The accuracy of the DP model stems from the distinctive ability of deep neural networks (DNN) to approximate high-dimensional functions [7, 40], the proper treatment of physical requirements like symmetry constraints, and the concurrent learning scheme that generates a compact training dataset with a guarantee of uniform accuracy within the relevant configuration space [68].

As shown in Fig. 1, to construct a DP model, first, the coordinates of an atom and its neighboring atoms are converted to the

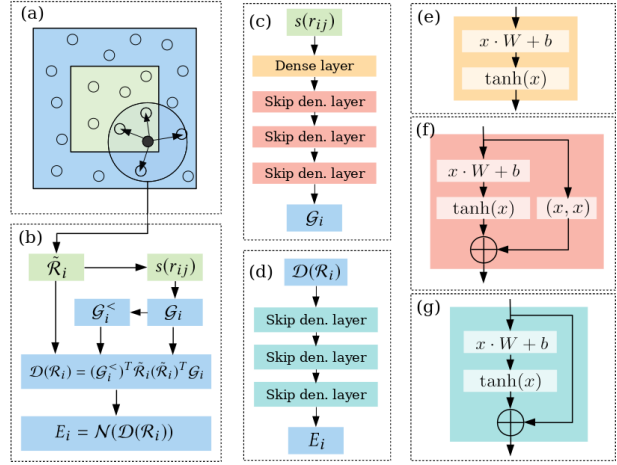


Figure 1: Schematic plot of the DP method. (a) A sub-region, including the local sub-region (green) and the ghost region (blue), handled by an MPI processor. (b) Mapping of the local environment of a single atom onto atomic energy contribution. (c) Structure of the embedding net. (d) Structure of the fitting net. (e) Dense layer used in the embedding net. (f) Skip connected dense layer used in the embedding net. (g) Skip connected dense layer used in the fitting net.

descriptors \mathcal{D} , which encode the local atomic environment by a group of symmetry preserving features and trainable parameters. Next, the descriptors are passed to the *fitting net*, a fully connected DNN denoted by \mathcal{N} , which outputs the atomic energy contribution E_i . Finally, the potential energy is constructed as the summation of E_i . In detail, the descriptor \mathcal{D} is the product of terms involving the *environment matrix* \mathcal{R} , which faithfully records the relative positions of the neighbors, and the *embedding matrix* \mathcal{G} , which encodes the information of the distances between atoms by a DNN named *embedding net*. The training of the DP model has been implemented in the DeePMD-kit package [60]. The typical training time spans from several hours to one week on a single GPU card, depending on the complexity of the data.

Deep Potential Molecular Dynamics (DeePMD) has greatly boosted the time and size scales accessible by AIMD without loss of *ab initio* accuracy. To date, DeePMD has been used to model various phenomena in chemistry [6, 17, 64, 65] and materials sciences [11, 20, 38, 41, 59]. For example, in a recent work [6], DeePMD was used to simulate the TiO_2 -water interface, providing a microscopic answer to an unsolved question in surface chemistry: do water molecules dissociate or remain intact at the interface between the liquid and TiO_2 ? In another recent work [11], DeePMD was used in combination with experiments to show the mechanism behind the nucleation of strengthening precipitates in high-strength lightweight aluminium alloys. These examples are challenging for AIMD to tackle due to the spatial and temporal limits. They are also hard, if not impossible, for EFF-based MD schemes, due to the limited capability of the relatively simple form of the potential energy function they adopt.

4 CURRENT STATE OF THE ART

An important goal of molecular simulation is to model with *ab initio* accuracy realistic processes that involve hundreds of millions of atoms. To achieve this goal, there have been tremendous efforts made for boosting AIMD without loss of its accuracy. Some examples are QBox [26], LD3DF [62], RSDFT [28], DFT-FE [21] and CONQUEST [44]. Their performance is summarized in Table 1, where the system size, the peak performance, the time-to-solution, etc., are provided. We observe that it is hard for conventional DFT-based AIMD schemes to overcome the limit of the cost even by the fastest HPCs nowadays. As a rough estimate, even if the development of HPC keeps the same speed as the past thirteen years, one has to wait for tens of years for HPC to be powerful enough to achieve the target system size within conventional AIMD techniques.

The MLMD schemes introduced in the last section offer a chance to bypass the conventional AIMD methods without losing its accuracy. Representative examples are the Behler-Parrinello scheme [10], the Gaussian approximation potential [8, 9], SchNet [51], the ANI model [54], and Deep Potential [27, 66]. Up to now, most attentions of the community have been paid to improving the representability and transferability of these machine learning based schemes, and on solving scientific problems that do not require really large-scale MD simulations. Efforts on implementation and optimization from an HPC perspective have been in an early stage. Some open-source packages for the MLMD schemes have been released: the QUantum mechanics and Interatomic Potentials (QUIP) [1], Amp [32], DeePMD-kit [60], TensorMol [63], SIMPLE-NN [35], PES-Learn [4], and a library-based LAMMPS implantation of neural network potential [53]. The performance reported by these work, if any, is summarized in Tab. 1. However, it is observed that the implementations of MLMD are basically for desktop GPU workstations or CPU-only clusters. None of them can fully utilize the computational power offered by the accelerators on modern heterogeneous supercomputers.

Of particular relevance to our work is the DeePMD scheme, which has been implemented by an open-source package called DeePMD-kit [60]. DeePMD-kit is built based on the an MD platform LAMMPS [45] and a deep learning platform TensorFlow [3]. By interfacing with LAMMPS, which maintains the atomic information and integrates the equation of motion, the key function of DeePMD-kit is to implement the calculation of atomic energies and forces predicted by the DP model. With TensorFlow, a versatile tool box for deep learning, the embedding matrix, descriptor, and the atomic energy are implemented by standard operators built in TensorFlow. Moreover, TensorFlow provides GPU support for its standard operators, thus the corresponding calculations in DeePMD-kit are easily accelerated with GPU by linking to the GPU TensorFlow library. Unfortunately, the implementation of DeePMD-kit cannot fully utilize the computational power of modern heterogeneous supercomputers like Summit, due to the following restrictions: (1) The code is designed on single node with only single GPU serial or multi-CPU OpenMP parallelism [60]. (2) The customized TensorFlow operators introduced for the environment matrix, force, and virial are implemented only on CPUs. (3) The size of the DNN used by DP models is relatively smaller than sizes adopted in typical

deep learning applications like pattern detection and language processing, which implies that each individual step of computationally intensive operation is also relatively smaller. In this context, the memory bandwidth and latency become obstacles to improving the computational efficiency of the DeePMD-kit package. To summarize, large-scale DeePMD simulations with *ab initio* accuracy have been only conceptually proved to be possible, but have never been made practically accessible by a code optimized for modern heterogeneous HPCs, from both algorithmic and implementation perspectives.

Above all, to the best knowledge of the authors, efficient MD simulation of 100 million atoms with *ab initio* accuracy has never been shown by AIMD or MLMD schemes. We believe that to make this goal a routine procedure, the way to pursue is to integrate physics-based modeling and simulation, machine learning, and efficient implementation on the next-generation computational platform. In the following sections, we shall adopt the serial DeePMD-kit [60] as the baseline DeePMD implementation, and we demonstrate how its performance is greatly boosted on the Summit.

5 INNOVATIONS

5.1 Summary of contributions

Our major contribution is a highly efficient, highly scalable method for performing MD simulation with *ab initio* accuracy. This is achieved by combining the unprecedented representation capability of the DP model (Fig. 2 (a)-(b)), and a highly scalable and fine-tuned implementation on heterogeneous GPU architectures (Fig. 2 (c)-(g)). The resulting optimized DeePMD-kit scales almost perfectly up to 4560 computing nodes on Summit for a copper system of 113,246,208 atoms, reaching 86 PFLOPS in double precision and 137 PFLOPS in mixed precision. The corresponding time-to-solution is 52 milliseconds per MD step, enabling nanosecond simulation within 15 hours. Our time-to-solution outperforms existing works by more than three orders of magnitude, and brings the molecular dynamics simulation with *ab initio* accuracy into a new era.

5.2 Algorithmic innovation

To effectively harness the computing power offered by the heterogeneous system architecture of Summit, our goal is to migrate to GPUs almost all computational tasks and a significant amount of communication tasks. Due to the relatively limited size of the computational granularity in the DP model, a straightforward GPU implementation can encounter many bottlenecks and is thus not efficient. As such, our main algorithmic innovations are as follows:

- We increase the computational granularity of DeePMD by introducing a new data layout for the neighbor list that avoids branching in the computation of embedding matrix.
- The elements in the new data structure of the neighbor list are compressed into 64-bit integers for more efficient GPU optimization of the customized TensorFlow operators.
- We develop the mixed-precision computation for the DP model. Computationally intensive tasks are performed with single precision without violating the accuracy of physical observables.

Table 1: Performance of molecular dynamics simulators with *ab initio* accuracy. The abbreviations Pot., VE, TtS, LS, BP, and DP stand for potential, valence electrons, time-to-solution, linear scaling, Behler-Parrinello scheme, and Deep Potential, respectively. In AIMD, we assume 5 electronic steps in each MD (ionic) step. The time step of water system is 0.5 fs, and that of other systems is 1 fs. *The parallel efficiency does not significantly decay at the largest machine scale tested in the work, so it is highly likely that they can scale to larger machines. †Vienna Scientific Cluster (VSC), an HPC system with Intel Xeon Gold 6138 CPUs. ‡An unknown cluster with Intel Xeon E5-2650v2 CPUs at the KISTI supercomputing center. **The baseline DeePMD-kit implementation.

Work	Year	Pot.	System	# VE	# atoms	# CPU cores	# GPUs	Machine	Peak[FLOPS]	TtS [s/step/atom]
Qbox [26]	2006	DFT	Mo	12K	1K	262K	–	BlueGene/L	207T	2.8×10^{-1}
LS3DF [62]	2008	LS-DFT	ZnTeO	?	16K	131K	–	BlueGene/P	108T	1.8×10^{-2}
RSDFT [28]	2011	DFT	Si	?	107K	442K	–	K-computer	3.1P	2.6×10^0
DFT-FE [21]	2019	DFT	Mg	105K	11K	159K	22.8K	Summit	46P	6.5×10^{-2}
CONQUEST [44]	2020	LS-DFT	Si	?	1M	200K	–	K-computer	?	4.0×10^{-3}
Simple-NN [35]*	2019	BP	SiO ₂	–	14K	80	–	VSC†	?	3.6×10^{-5}
Singraber el.al. [53]*	2019	BP	H ₂ O	–	9K	512	–	Unknown‡	?	1.3×10^{-6}
Baseline [60]**	2018	DP	H ₂ O	–	25K	1	1	Summit	–	5.6×10^{-5}
This work	2020	DP	H ₂ O	–	403M	27.3K	27.3K	Summit	73P	2.7×10^{-10}
This work	2020	DP	Cu	–	113M	27.3K	27.3K	Summit	86P	7.3×10^{-10}

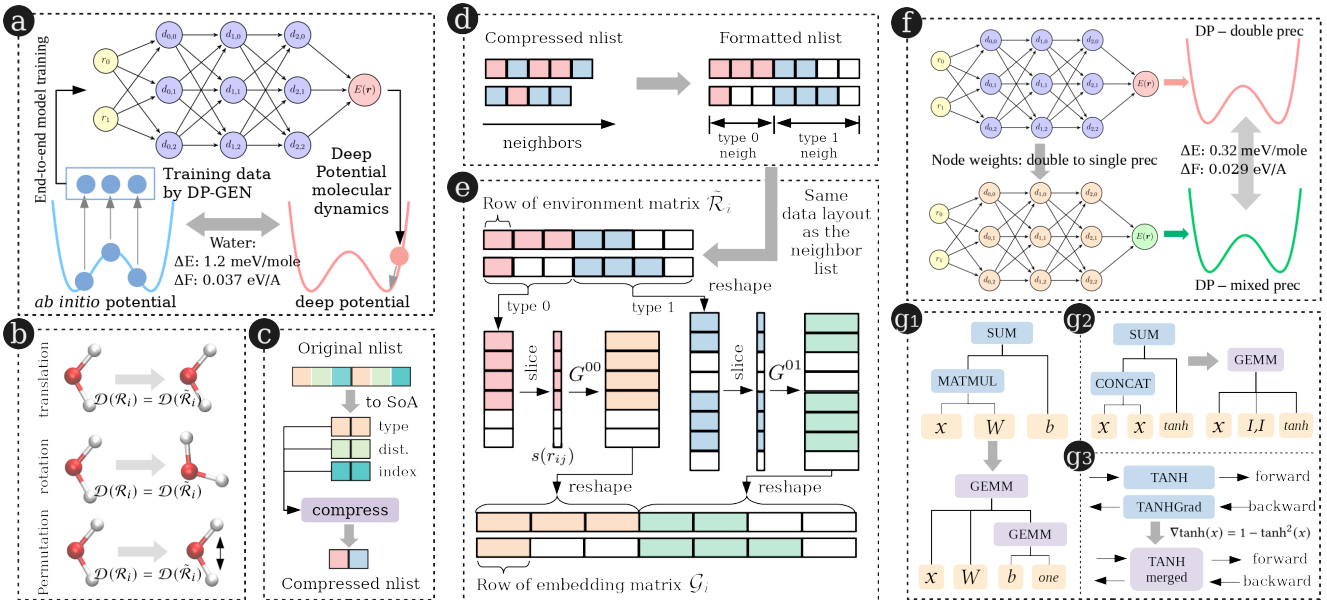


Figure 2: Key steps in the optimized DeePMD-kit, taking water as an example.

5.2.1 Increasing computational granularity. The novelty of the DP model lies in automatically generating a set of symmetry-preserving descriptors \mathcal{D} through the embedding net (Fig. 1 (b) and (c)) from the local environment of each atom described by the environment matrix \mathcal{R}_i . By using roughly the same set of hyper-parameters, our method can fit the data for almost all systems. Compared to other methods with fixed feature sets, DeePMD-kit is more stable when facing complex data, e.g., multi-component systems, chemical reactions, etc. Since important symmetries are strictly preserved in

\mathcal{D} (see Fig. 2 (b)), a fitting network of three layers (see Fig. 1 (d)) is already enough to produce results with high fidelity.

The most computationally intensive part of the DP model is the embedding matrix. The pattern of the computation is defined by the order of neighbors recorded in the neighbor list. We notice that since the descriptors are permutationally invariant (Fig. 2 (b)), the neighbor lists with any order are equivalent in terms of accuracy. By taking this advantage, we redesign the data layout of the neighbor list by sorting the neighbors according to their type, and, within each type, we sort the neighbors by their relative distance. The

neighbors of the same type are padded to the cut-off number of neighbors of that type (Fig. 2 (d)). The first sorting (according to neighbor types) and the padding align the neighbors with the same type, so the conditional branching according to the neighbor type in the embedding matrix computation is avoided (see Fig. 2 (e)). This greatly increases the computational granularity, a critical component for taking advantage of the computational power offered by GPUs. The second sorting always selects the nearest neighbors to the neighbor list, so that unphysical phenomena are avoided when the number of neighbors of a certain type occasionally fluctuates beyond the cut-off number of neighbors defined in the padding step.

5.2.2 Optimization of Customized TensorFlow Operators. In this part, we present the optimization of the customized TensorFlow operators, which take more than 84% of the total computational cost in the baseline DeePMD-kit. We start from formatting the neighbor list, whose data layout is crucial and discussed in Sec. 5.2.1. Each element of the neighbor list is a structure with 3 data items: the atomic type $\alpha(j)$, the atomic distance $|r_{ij}|$ and the atomic index j (Fig. 2 (c)). In the formatting process, the neighbor list is sorted first based on the atomic type, then based on the atomic distance $|r_{ij}|$.

The AoS (Array of structures) data layout of the neighbor list makes it impossible for efficient memory access on GPU because of memory coalescing problems. One common practice in GPU optimization is to switch from AoS to SoA (Structure of arrays). However, in DeePMD-kit, we propose an even more efficient way of storing the neighbor list by compressing each element of the neighbor list into a 64-bit integer (Fig. 2 (c)) with the following equation: $\alpha(j) \times 10^{15} + \lfloor |r_{ij}| \times 10^8 \rfloor \times 10^5 + j$. The 19 digits of an unsigned long long integer are divided into 3 parts to store the one element of neighbor list: 4 digits for the atomic type, 10 digits for the atomic distance, and 5 digits for the atomic index. The range of all the three parts are carefully chosen and are rarely exceeded in typical DeePMD simulations. Both the compression before sorting and the decompression after sorting are accelerated via CUDA customized kernels, so that the corresponding computational time is negligible. Sorting the compressed neighbor list reduces the number of comparisons by half with no impact on the accuracy of the algorithm, and is carried out by calling the NVIDIA CUB library, which provides the state-of-the-art and reusable software components for each layer of the CUDA programming model, including block-wide sorting.

According to Amdahl’s law, an ideal overall speedup can only be achieved by accelerating all calculations. In our implementation, all customized TensorFlow operators, Environment, ProdForce and ProdViral, which compute the environment matrix, force and the virial, respectively, are migrated and optimized on the GPU. In particular, a fine grain parallelism is utilized to exploit the computing power of the GPU.

Now that all computationally intensive tasks are carried out by the GPU, we further reduce the time for GPU memory allocation by allocating a trunk of GPU memory at the initialization stage, and re-using the GPU memory throughout the MD simulation. The CPU-GPU memory copy operations are also optimized to eliminate non-essential data transfer processes.

5.2.3 Mixed-precision computation. The approximation property of the DNN-based DP model provides us with an opportunity for mixed-precision calculations. In the optimized code, different levels of mixed precision are tested, and we find that a stable and accurate prescription is to use single precision for all the network parameters, but use double precision for other parts like the atomic positions and energies. In detail, the environment matrix, constructed in double precision, is converted to single precision and then is used to predict atomic energy and force by DNNs in single precision. Finally the results are converted from single precision back to double precision, and the total energy of the system is reduced from the atomic contributions.

We compare the mixed with the double precision model by using a typical configuration of a water system composed of 4,096 molecules, and observe a deviation of 0.32 meV/molecule in the energy prediction and a root mean square deviation of 0.029 eV/Å in the force predictions. Since these deviations are less than the training error of the double precision model, the mixed precision implementation is of satisfactory accuracy. In terms of speed and GPU memory requirement, the mixed precision is ~ 1.5 times faster than and consumes $\sim 50\%$ less memory than the double precision version. We remark that although half precision is more power efficient on the NVIDIA V100 GPU than single precision (120 TFLOPS against 14 TFLOPS), our tests show that, due to the limited representation range with 16 binary bits, the corresponding DP model cannot preserve the required accuracy of the energy and forces. Therefore, at this moment, we cannot take advantage of the merits of the half-precision implementation.

5.3 Neural Network Innovation

After optimizing customized TensorFlow operators (Sec. 5.2.2), the remaining computational cost is dominated by standard TensorFlow operators. The floating point operations are dominated by operators like MATMUL (matrix-matrix multiplication) and TANH (activation function). Other operators such as CONCAT (matrices concatenation) and SUM (matrix addition) are bandwidth intensive and cost few floating point operations. We find that many operations in DeePMD-kit involve matrix-matrix multiplication of tall and skinny matrices. This leads to particularly large overheads in the operations such as SUM operation, and hence standard TensorFlow operators are not optimized to treat such matrices efficiently. Through detailed performance profiling, we redesign the execution graph of TensorFlow as follows. Although these are tailored operations designed to improve the efficiency of DeePMD-kit, similar strategies should be useful in other machine learning applications, particularly those integrated with physical modeling.

5.3.1 Replace MATMUL and SUM Operators with GEMM. In the standard TensorFlow execution graph, the operation $x \cdot W + b$ (see Fig. 1 (e-g)) is implemented with two separate operators: MATMUL and SUM. For example, for the oxygen-hydrogen pairs in a water system with 4,096 molecules, MATMUL multiplies x of size 376,832 by 50 with W of size 50 by 100. Then the SUM operator adds the bias b to each row of $x \cdot W$. In most applications the sizes of matrices x and W are large enough so that the overhead of the SUM is negligible compared to that of the MATMUL operator. However, in the case of DeePMD, the second dimension of x and the size of W

are relatively small, so the cost of SUM becomes important. In the optimized computational graph, we replace MATMUL and SUM operators with a single CUBLAS GEMM call ($C = \alpha A \times B + \beta C$). Note that the vector b is converted to a matrix before SUM by right multiplying with the transpose of vector *one* (Fig. 2 (g1)).

5.3.2 Replace CONCAT and SUM Operators with GEMM. In the standard TensorFlow computational graph the operation $(x, x) + \dots$ (see Fig. 1 (f)) is implemented by a CONCAT operator that concatenates two x s to form (x, x) and a SUM operator that adds (x, x) with the output of the TANH operator. We optimize this operation by replacing CONCAT with a matrix-matrix multiplication $(x, x) \rightarrow x \times (I, I)$, and merging this multiplication with SUM to form a CUBLAS GEMM call (Fig. 2 (g2)). We observe that the multiplication is only marginally faster than CONCAT, and the benefit comes from the merging of the SUM.

5.3.3 CUDA kernel fusion for the TANH and TANHGrad. TANH is the activation function (see Fig. 1 (e-g)), while TANHGrad (not explicitly shown in Fig. 1) is the derivative of the output of TANH w.r.t the input for backward propagation. We need both TANH and TANHGrad in each MD step to evaluate the energy and forces. We observe that the derivative of $\tanh(x)$ is also a function of $\tanh(x)$, i.e. $\nabla \tanh(x) = 1 - \tanh^2(x)$. Thus, in the optimized DeePMD-kit, both TANH and TANHGrad operators are implemented in one CUDA customized kernel to save computational time (Fig. 2 (g3)). Since the GPU memory of the TANHGrad is allocated in the forward propagation, this optimization is essentially trading space for time.

5.4 Reducing MPI communication bottlenecks

Despite the multi-body nature of DP, due to the force decomposition scheme developed by us, we can adopt for DP the same parallelization scheme of the EFFs implemented in LAMMPS (Fig. 1 (a)). We thus replace the computation of EFFs in LAMMPS by the computation of DP, and use LAMMPS to maintain the spacial partitioning of the system and all the communications between sub-regions.

There are mainly two types of MPI communications in each DeePMD step: the communication of the ghost region between adjacent MPI tasks and the global reduction for the physical properties. In our implementation, we optimize the communication of the ghost region using the CUDA-aware IBM Spectrum MPI, since it resides on the GPU in the calculation. When output information is required, *MPI_Allreduce* operations across all MPI tasks are performed to collect physical properties such as total energy, stress, etc.. Although each of these physical properties is only one double precision number and the corresponding *MPI_Allreduce* operation is latency dominated, the scaling of the optimized DeePMD-kit is hindered by the implicit *MPI_Barrier* in extremely large-scale calculations. To alleviate this problem, we reduce the output frequency to every 20 steps, a common practice in the MD community. In addition, we replace the *MPI_Allreduce* with *MPI_Iallreduce* to further avoid the implicit *MPI_Barrier*.

6 PERFORMANCE MEASUREMENT

6.1 Physical Systems

Among various complex physical systems that have been described by DP, we choose two typical and well-benchmarked systems, one

insulating (water) and one metallic (copper), to measure the performance of the optimized DeePMD-kit. Water is a notoriously difficult system even for AIMD, due to the delicate balance between weak non-covalent intermolecular interactions, thermal (entropic) effects, as well as nuclear quantum effects [15, 22, 33]. We have shown in Refs. [33, 66] that DeePMD can accurately capture such effects in water. In combination with extensions of the DP formulation to vectors and tensors, the infra-red [65] and Raman [55] spectra of water have been properly described. Copper is a representative simple metal, yet a lot of its properties, such as the surface formation energy and stacking fault energies, can be hardly produced well by EFFs. In Ref. [69], using a concurrent learning scheme [68], we have generated a minimal set of *ab initio* training data and realized a DP model for copper with a uniform accuracy over a large thermodynamic region.

For water and copper, the cut-off radii are 6 Å and 8 Å and the cut-off numbers of neighbors are 138 and 500, respectively. The fitting nets of the models are of size $240 \times 240 \times 240$, and the embedding nets are of size $25 \times 50 \times 100$. To test the performance, the MD equations are numerically integrated by the Velocity-Verlet scheme for 500 steps (the energy and forces are evaluated for 501 times) at time-steps of 0.5 fs (water) and 1.0 fs (copper). The velocities of the atoms are randomly initialized subjected to the Boltzmann distribution at 330 K. The neighbor list with a 2 Å buffer region is updated every 50 time steps. The thermodynamic data, including kinetic energy, potential energy, temperature, pressure, are collected and recorded in every 20 time steps.

For the water systems, the strong scaling tests are performed on a system with 4, 194, 304 molecules (12, 582, 912 atoms). The total number of floating point calculation for 500 MD steps of this system is 124.83 PFLOPs. Weak scaling tests ranging from 25, 165, 842 to 402, 653, 184 atoms are performed on up to 4560 computing nodes on Summit. We notice that compared to the water system, the copper system can be 3.5 times bigger both in terms of floating point operations and GPU memory footprint under the same number of atoms. The strong scaling tests of the copper system are carried out with a system of 25, 739, 424 atoms. The total number of floating point calculation for 500 MD steps of this system is 835.53 PFLOPs. The weak scaling tests are performed on up to 4560 computing nodes of Summit for systems ranging from 14, 155, 776 to 113, 246, 208 atoms.

Since the baseline DeePMD-kit is restricted by its sequential implementation and can run neither of these systems, a fraction of the water system (12, 288 atoms/4096 water molecules) is used for comparison with the optimized code on a single GPU in Sec. 7.1.

6.2 HPC Platforms and Software Environment

All the numerical tests are performed on the Summit supercomputer, which is consisted of 4608 computing nodes and ranks No. 1 on the TOP500 list for a peak performance of 200 PFLOPS [2]. Each computing node has two identical groups, each group has one POWER 9 CPU socket and 3 NVIDIA V100 GPUs and they are interconnected via NVLink. The total computing power for a single node is 43 TFLOPS in double precision (each V100 GPU 7 TFLOPS and each POWER 9 socket 515 GFLOPS, thus $7 \times 6 + 2 \times 0.5 = 43$ TFLOPS in total) and 86 TFLOPS in single precision. We remark that

6 V100 GPUs provide 720 TFLOPS half precision computing power with Tensor cores, but they are not used in our tests due to accuracy problem. Each computing node has 512GB host memory and 96GB (16GB per GPU) GPU memory. The CPU bandwidth is 135GB/s (per socket) and GPU bandwidth is 900GB/s (per GPU). The two groups of hardware are connected via X-Bus with a 64GB/s bandwidth. The computing nodes are interconnected with a non-blocking fat-tree using a dual-rail Mellanox EDR InfiniBand interconnect with a total bandwidth of 25GB/s.

Table 2: Software environment

Name	Module used
MPI	IBM Spectrum MPI 10.3.1.2-20200121
Host compiler	GCC 4.8.5
GPU compiler	CUDA 10.1.168
TensorFlow	IBM-WML-CE 1.6.2-2 (TensorFlow 1.15 included)

The software environment is listed in Table 2. In all tests, single OpenMP thread is used. We use 6 MPI tasks per computing node (3 MPI tasks per socket to fully take advantage of both CPU-GPU affinity and network adapter), and each MPI task is bound to an individual GPU.

6.3 Measurements

The total number of floating point operations (FLOPs) of the systems is collected via NVIDIA CUDA NVPYPROF tool. We remark that NVPYPROF only gathers the FLOPs on the GPU. However, in DeePMD-kit, all computationally intensive calculations are performed on the GPU, thus the total FLOPs is reasonable. Both double-precision and mixed-precision results are reported in Sec. 7. The following three criteria are used to measure the performance of the DeePMD-kit.

- **Time-to-solution**, defined as the average wall clock time used in calculating a single MD steps, and calculated by $\frac{\text{MD loop time}}{\text{number of MD steps}}$. The “MD loop time” includes all the time used in the MD loop (IO included). Setup time, such as the setup of the system and MPI initialization and finalization, is not included.
- **Peak performance**, defined as $\frac{\text{total FLOPs}}{\text{MD loop time}}$.
- **Sustained performance**, defined as $\frac{\text{total FLOPs}}{\text{total wall clock time}}$. The “total wall clock time” includes the whole application running time (including IO).

7 PERFORMANCE RESULTS

7.1 Single GPU

In this part, we show the performance of the individual components, including the customized TensorFlow operators, the standard TensorFlow operators, and the total performance of a single GPU on Summit.

7.1.1 Customized TensorFlow operators. We optimize the customized TensorFlow operators with CUDA customized kernels according to Sec. 5.2.2. In the baseline implementation, the customized TensorFlow operators take about 85% of the total MD loop time for a

Table 3: Performance of optimized customized TensorFlow operators. Baseline customized operators are implemented on CPU.

Operators	Baseline[ms]	Optimized[ms]	Speedup
Environment	302.54	2.32	130
ProdViral	51.06	1.34	38
ProdForce	41.29	2.41	17

water system of 12,288 atoms. The performance of the customized operators of the baseline and optimized implementations are compared in Tab. 3. For all the customized TensorFlow operators, an overall speedup of 64.6 times is achieved. Moreover, a total speedup factor of 6.2 is reached for the “MD loop time”.

7.1.2 Standard TensorFlow operators. The standard TensorFlow operators are re-implemented and optimized according to Sec. 5.3. For the water system of 12,288 atoms, MATMUL+SUM, CONCAT+SUM and TANH+TANHGrad in the baseline implementation are accelerated by 1.3, 1.7 and 1.6 times with GEMM, GEMM and merged TANH in the optimized implementation, respectively. We remark that the baseline implementation calls standard TensorFlow operators, which are already highly efficient on GPUs, yet an extra 1.21 times of speedup is achieved for the “MD loop time” compared with Sec. 7.1.1.

Fig. 3 shows the percentage of time spent by different TensorFlow operators in the total GPU execution time. We notice that the contribution from the GEMM operator is more important in the copper system (double:74%, mixed:72%) than that in the water system (double:63%, mixed: 62%). This is mainly attributed to two reasons: First, copper is a monoatomic system, thus the corresponding bandwidth intensive TensorFlow operators like sorting and slicing are not needed. Second, the FLOPs of the copper system is 3.5 times bigger than that of the water due to the larger number of neighbors per atom, as discussed in Sec. 6.1. We remark that the GEMM operator in DeePMD-kit is still memory-bound due to the small network size (the dimensions of the three fitting network layers are in 25,50 and 100). Profiling on the water system shows that the double-precision efficiency of the GEMM associated with the fitting network (dimension 25,50 and 100) is 52.86%, 64.08% and 71.17%, respectively. The corresponding bandwidth utilization is 73%, 63% and 38% of the hardware limit.

7.1.3 Mixed precision. We compare the prediction of the mixed precision model with that of the double precision model for a water system with 4,096 molecules. Deviations of 0.32 meV (normalized by number of molecules) in energy and 0.029 eV/Å in forces are observed. Both the deviations are essentially smaller than the prediction error of the double precision model compared with *ab initio* data. To further check the accuracy, we calculate the radial distribution function (RDF), the normalized probability of finding a neighboring atom at the spherically averaged distance r . The oxygen-oxygen ($g_{OO}(r)$), oxygen-hydrogen ($g_{OH}(r)$), and hydrogen-hydrogen ($g_{HH}(r)$) RDFs are typically utilized to characterize the structures of water [66], and they are compared in Fig. 4. The RDFs computed from the mixed-precision implementation

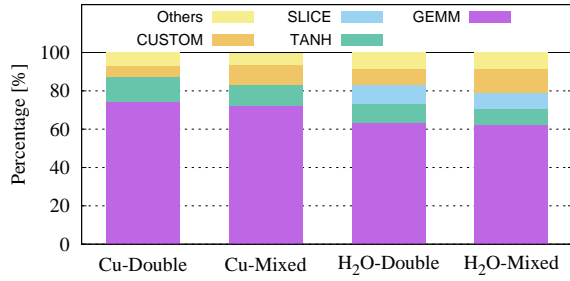


Figure 3: Percent stacked bar chart of different TensorFlow operators in terms of the GPU computational time.

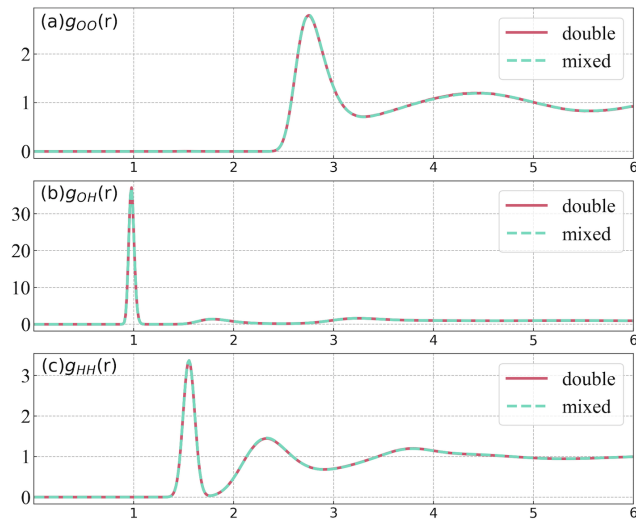


Figure 4: Radius distribution functions $g_{OO}(r)$, $g_{OH}(r)$, and $g_{HH}(r)$ of liquid water consisting of 12,288 atoms at ambient conditions, calculated by MD simulations using the double-precision version and mixed-precision version of the optimized DeePMD-kit.

agree perfectly with those from the double-precision implementation. Therefore, we conclude that the mix-precision method does not lead to loss of accuracy in computing physical observables.

The mixed-precision code is about 1.5 times faster, and saves half of the GPU memory cost, compared to the double-precision version. Together with the speedups from Secs. 7.1.2 and 7.1.1, it is concluded that the optimized DeePMD-kit with double precision is estimated to be 7.5 times faster than the baseline code, and the speedup factor increases to 11.3 when the mixed precision is used.

7.2 Scaling

We discuss the scaling behaviors of the optimized DeePMD-kit on the Summit supercomputer for large-scale simulations. The system sizes, ranging from 12 to 402 million of atoms, are inaccessible by the baseline implementation, and are more than two orders of

magnitude larger than other state-of-the-art MD schemes with *ab initio* accuracy.

7.2.1 Strong Scaling. In Fig. 5, we measure the scalability of the optimized DeePMD-kit with the “MD loop time” of 500 MD steps ranging from 80 to 4560 computing nodes. The testing systems include a water system of 12,582,912 atoms and a copper system of 25,739,424 atoms.

For the copper system, the optimized DeePMD-kit scales well to the entire Summit supercomputer. By setting the performance with 570 computing nodes as baseline, the parallel efficiency is 81.6% and 70.5% when scaling to 4560 computing nodes on Summit, **reaching peak performance of 76.4 PFLOPS and 107.8 PFLOPS for the double and mixed precision versions of the code, respectively**. The time-to-solution of a single MD step for this particular system is 15 milliseconds using the mixed-precision version of optimized DeePMD-kit, making it possible to finish nanosecond simulation within 4.2 hours with *ab initio* accuracy.

For the water system, the optimized DeePMD-kit scales almost perfectly up to 640 computing nodes, and continues to scale up to the entire Summit supercomputer. Compare to the baseline of 80 computing nodes, the parallel efficiency of the optimized DeePMD-kit is 84.7%(double) and 76.8%(mixed) when scaling to 640 computing nodes, and decreases to 36%(double) and 27.6%(mixed) when using 4560 computing nodes. The decrease of the parallel efficiency is mainly due to the scaling of the data size per GPU. As shown in Table 4, the percentage of peak performance goes down dramatically when the number of atoms per GPU is less than 1,000. However, we remark that both double and mixed precision versions of DeePMD-kit scale up to 4560 computing nodes with 459 atoms per GPUs despite the small data size. **The time-to-solution of a single MD step for this system with double-precision is 9 milliseconds, making it possible to finish nanosecond simulation in 5.0 hours (time step is 0.5 fs).**

Table 4: Average number of atoms (per GPU), average ghost region size (per GPU), and double precision FLOPS for the 12,582,912 atoms water system.

#GPUs	480	960	1920	3840	7680	15360	27360
#atoms	26214	13107	6553	3276	1638	819	459
#ghosts	25566	16728	11548	7962	5467	3995	3039
MD time	92.31	47.11	25.08	13.62	7.98	5.76	4.53
Efficiency	1.00	0.98	0.92	0.85	0.72	0.50	0.36
PFLOPS	1.35	2.65	4.98	9.16	15.63	21.66	27.51
% of Peak	38.54	37.76	35.46	32.64	27.85	19.30	13.75

7.2.2 Weak scaling. The weak scaling of the optimized DeePMD-kit is measured in terms of the FLOPS of 500 MD steps for both water and copper (Fig. 6). Both systems show perfect scaling with respect to the number of nodes (GPUs) used. The mixed-precision version is about 1.5 times faster compared to the double-precision code in all tests. For water and copper, the largest system sizes simulated in these tests are 403 and 113 million atoms, respectively, which are more than two orders of magnitude larger compare to the state-of-the-art MD with *ab initio* accuracy. For the copper system, **the peak**

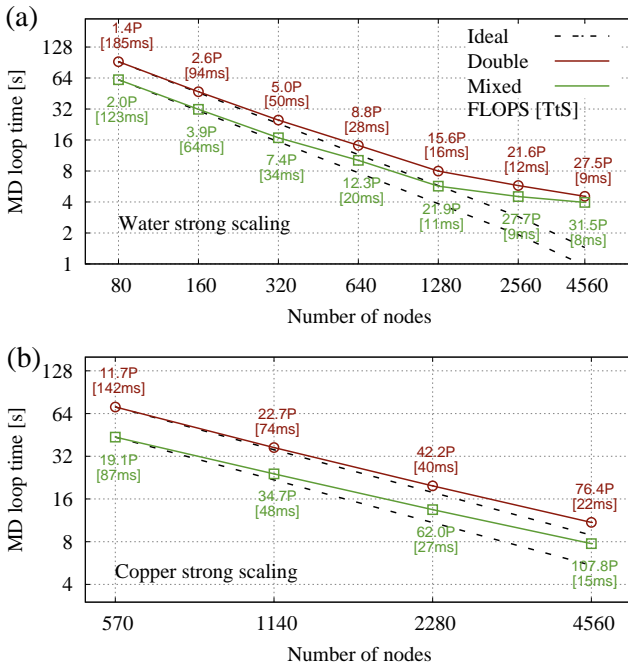


Figure 5: Strong scaling: (a) the water system of 12,582,913 atoms (b) the copper system of 25,739,424 atoms. The copper system is about 7 times larger than the water system in terms of both floating point operations and memory usage. The loop time is counted by MD simulations of 500 time steps (energy and forces are computed 501 times). The corresponding peak performance in PFLOPS and the time-to-solution (TtS) in millisecond per MD step are presented.

performance achieved is 86.2 PFLOPS (43% of the peak) in double precision and 137.4 PFLOPS in mixed precision. The time-to-solution is 7.3×10^{-10} second/step/atom in double precision, and 4.6×10^{-10} second/step/atom in mixed precision, which means that one nanosecond MD simulation of the 113M-atom system with *ab initio* accuracy can be finished in 23 and 14 hours (1.0 fs time step), respectively. For the water system, the peak performance is 72.6 PFLOPS (36% of the peak) in double precision and 105.4 PFLOPS in mixed precision. The optimized code reaches a time-to-solution of 2.7×10^{-10} second/step/atom in double precision and 1.8×10^{-10} second/step/atom in mixed precision. Thus one nanosecond MD simulation of the 403M-atom water system with *ab initio* accuracy can be finished in 61 and 24 hours (0.5 fs time step), in double and mixed precision, respectively. We remark that the perfect linear scaling of both systems implies that the optimized DeePMD-kit is able to calculate even bigger physical systems on future exascale supercomputers with no intrinsic obstacles.

7.3 Sustained performance

The MD loop time of the optimized DeePMD-kit has been measured and discussed in detail in Secs. 7.1 and 7.2. By subtracting the MD loop time from the total wall clock time, we define the “setup time”,

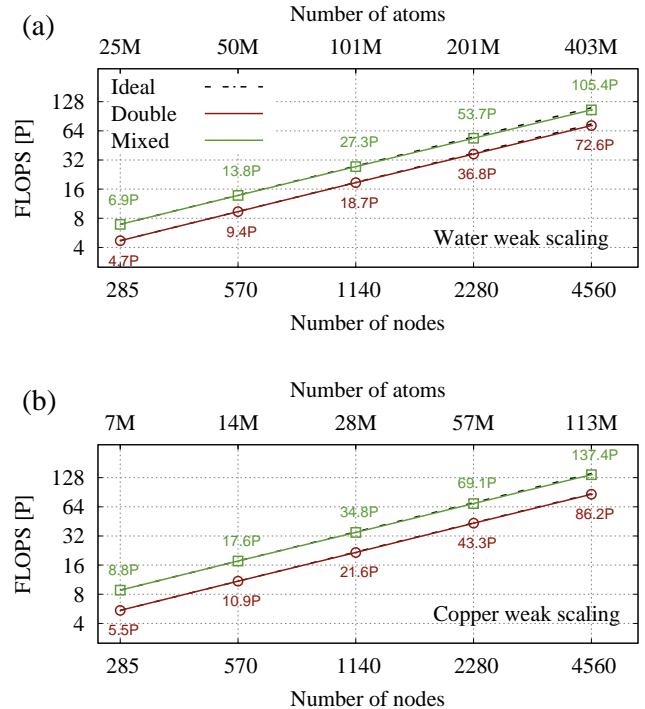


Figure 6: Weak scaling: (a) the water system. Number of atom ranges from 25,165,824 to 402,653,184. (b) the copper system. Number of atoms ranges from 7,077,888 to 113,246,208.

which mainly includes the initialization of the atomic structure and the loading of the DP model data. In the baseline implementation, the atomic structure is constructed on a single MPI task and then distributed via MPI communication, and the model data is read in from the hard-drive by all the MPI tasks. The corresponding setup time can be minutes, even though they are performed only once. For example, the setup time for the copper system of 113,246,208 atoms is more than 240 seconds on 4560 computing nodes on Summit.

To reduce these overheads, we build the atomic structure with all the MPI tasks without communication, and the model data is also staged by first reading in with a single MPI rank, and then broadcasting across all MPI tasks. By these optimizations, the setup time is reduced to less than 5 seconds for all tests. **The sustained performance of the DeePMD-kit reaches 85.4 PFLOPS in double precision when running the 113,246,208 atoms copper system for 5,000 MD steps (5 ps).** The time-to-solution is 7.4×10^{-10} second/step/atom, equivalent to 23 hours for a one-nanosecond simulation.

8 IMPLICATIONS

This work opens a new era in large-scale molecular dynamics simulation with *ab initio* accuracy. This unprecedented power results from integrating physics-based modeling and simulation, machine learning, and efficient implementation on the largest computational platform. It makes possible direct study of various problems, as

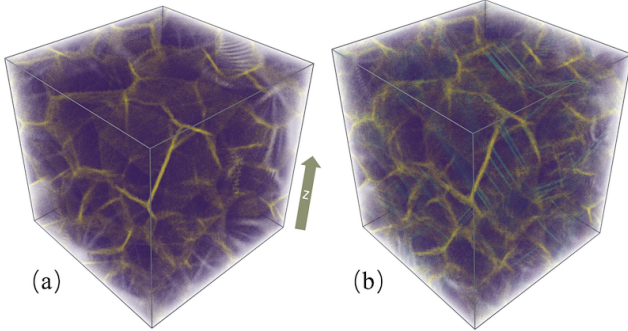


Figure 7: (a) A 10,401,218-atom nanocrystalline copper consisting of 64 randomly oriented crystals with 15-nm averaged grain diameter. (b) The nanocrystalline copper after 10% tensile deformation along the z axis. Purple, yellow, and cyan denote the atoms in the grains, atoms in the grain boundaries, and atoms in the stacking faults.

we introduce in Sec. 8.1, and it also poses new challenges to the next-generation supercomputer for a better integration of machine learning and physical modeling, as detailed in Sec. 8.2.

8.1 Applications of Optimized DeePMD-kit

The strength and hardness of metals can be enhanced by refining their grains, and MD can be of great help to provide microscopic insights into the underlying mechanism [49, 50]. Typically, a nanocrystalline structure of metal consists of tens to hundreds of millions of atoms [49, 50], which is far beyond the capability of *ab initio* methods. Therefore, previous simulation of nanocrystalline metals can only be driven by EFFs with limited accuracy. Taking copper as an example, EFFs are able to yield the strain-stress curves of nanocrystalline, from which the movements of dislocations and grain boundaries can be analyzed to elucidate the origins of strength in nanocrystalline. However, the biggest problem of EFFs is the lack of accuracy for certain properties, e.g., surface formation energies and stacking fault energies. The accuracy problem is largely resolved by the DP model used in this work. We refer to Ref. [69] for extensive benchmark.

We show in Fig. 7 the tensile deformation of a 10,401,218-atom nanocrystalline copper by MD simulations. The initial cell size is set to $50 \times 50 \times 50 \text{ nm}^3$. We run 50,000 steps with a time step of 0.5 fs. The first 10,000 steps are used for annealing at 300 K while the remaining 40,000 steps follow a strain rate of $5 \times 10^8 \text{ s}^{-1}$. In total, the nanocrystalline copper is deformed by 10%. We adopt the common neighbor analysis (CNA) scheme [19, 30] to analyze the structure of nanocrystalline copper. As shown in Fig. 7, the atoms in the grains has a face-centered cubic (fcc) local structure, which is the ground-state structure of copper. After the deformation, stacking faults of copper are identified by monitoring the formation of hexagonal close-packed (hcp) structures. The above example demonstrates the dynamical tensile deformation process of a nanocrystalline copper system. We leave the detailed analysis to a future paper that is dedicated to the physics of this process.

We expect that applications enabled by the multi-GPU implementation of the DeePMD-kit code can go far beyond copper and water systems reported here, and can span a wide spectrum of complex materials and molecules. This first stems from the wide applicability of the DP method to problems in different fields. Being a general model based on both machine learning and physics, DP inherits the accuracy from first-principles methods and puts on an equal footing the description of atomic interaction in the cases of bio-molecules, insulators, metals, and semi-metals, etc. This ability of DP is further boosted by this work, which takes advantage of the state-of-the-art supercomputers, and make simulation of hundreds of millions of atoms with *ab initio* accuracy a routine procedure. In the short term, this will direct benefit the study of many problems of practical interests, such as complex chemical reactions [37, 43], electrochemical cells [31], nanocrystalline materials [39, 49, 50], irradiation damages [25], and dynamic fracture and crack propagation [57, 58], etc., for which a very high accuracy and a system size of thousands to hundreds of millions of atoms, or even larger, is often required. In a longer term, this could be used to problems that are of a more significant practical interest, such as drug design and materials design.

8.2 Outlook in the era of Exascale computing

The past decade has witnessed the rapid growth of the heterogeneous architecture due to its superior performance in FLOPS per watt and memory bandwidth. This essentially requires a revisit of the scientific applications and a rethinking of the optimal data layout and MPI communication at an algorithmic level, rather than using GPUs purely as accelerators by offloading computational intensive tasks. In this paper, the critical data layout in the DeePMD method is redesigned to increase the task granularity, then the entire DeePMD-kit code is parallelized and optimized to improve its scalability and efficiency on the GPU supercomputer Summit. The optimization strategy presented in this paper can also be applied to other heterogeneous architectures, for example, it can be easily converted to the Heterogeneous-compute Interface for Portability (HIP) programming model to run on the next exascale supercomputer Frontier, which will be based on AMD GPUs. Based on the scaling shown in Fig. 6, we see no intrinsic obstacles to scaling our code to run on the exascale supercomputer for systems with billions of atoms. Compared to the traditional numerical methods such as density functional theory, one advantage of the deep potential lies in its resilience to numerical noises, which could significantly reduce the amount of work needed for fault-tolerant treatments. Therefore, methods like DeePMD can be ideal candidates in the upcoming era of exascale computing. On the other hand, improvements on the hardware, especially reducing the latency of GPU and network, are required to achieve better strong scaling for the DeePMD-kit on the next generation supercomputers.

ACKNOWLEDGMENTS

Numerical tests were performed on the Summit supercomputer located in the Oak Ridge National Laboratory. This work was partially supported by the National Science Foundation under Grant No. 1450372, No. DMS-1652330 (W. J. and L. L.), and by the Department of Energy under Grant No. DE-SC0017867 (L. L.). The work

of H. W. is supported by the National Science Foundation of China under Grant No. 11871110, the National Key Research and Development Program of China under Grants No. 2016YFB0201200 and No. 2016YFB0201203, and Beijing Academy of Artificial Intelligence (BAAI). We thank a gift from iFlytek to Princeton University and the ONR grant N00014-13-1-0338 (L. Z. and W. E), and the Center Chemistry in Solution and at Interfaces (CSI) funded by the DOE Award DE-SC001934 (L. Z., R. C. and W. E). The authors would like to thank Junqi Yin, Lin-Wang Wang, and Chao Yang for helpful discussions.

REFERENCES

- [1] [n. d.]. QUIP - QUantum mechanics and Interatomic Potentials. <https://github.com/libAtoms/QUIP>. Accessed: 2020-03-03.
- [2] [n. d.]. Top500 List, <https://www.top500.org>.
- [3] Martin Abadi, Paul Barham, Jianmin Chen, Zhifeng Chen, Andy Davis, Jeffrey Dean, Matthieu Devin, Sanjay Ghemawat, Geoffrey Irving, Michael Isard, et al. 2016. Tensorflow: A system for large-scale machine learning. In *12th {USENIX} Symposium on Operating Systems Design and Implementation ({OSDI} 16)*. 265–283.
- [4] Adam S Abbott, Justin M Turney, Boyi Zhang, Daniel GA Smith, Doaa Altarawy, and Henry F Schaefer. 2019. PES-Learn: An Open-Source Software Package for the Automated Generation of Machine Learning Models of Molecular Potential Energy Surfaces. *Journal of Chemical Theory and Computation* (2019).
- [5] Maral Aminpour, Carlo Montemagno, and Jack A Tuszynski. 2019. An Overview of Molecular Modeling for Drug Discovery with Specific Illustrative Examples of Applications. *Molecules* 24, 9 (2019), 1693.
- [6] Marcos F Calegari Andrade, Hsin-Yu Ko, Linfeng Zhang, Roberto Car, and Annabella Selloni. 2020. Free energy of proton transfer at the water-TiO₂ interface from ab initio deep potential molecular dynamics. *Chemical Science* (2020).
- [7] Andrew R Barron. 1993. Universal approximation bounds for superpositions of a sigmoidal function. *IEEE Transactions on Information theory* 39, 3 (1993), 930–945.
- [8] Albert P Bartók, Risi Kondor, and Gábor Csányi. 2013. On representing chemical environments. *Physical Review B* 87, 18 (2013), 184115.
- [9] Albert P Bartók, Mike C Payne, Risi Kondor, and Gábor Csányi. 2010. Gaussian approximation potentials: The accuracy of quantum mechanics, without the electrons. *Physical Review Letters* 104, 13 (2010), 136403.
- [10] Jörg Behler and Michele Parrinello. 2007. Generalized neural-network representation of high-dimensional potential-energy surfaces. *Physical Review Letters* 98, 14 (2007), 146401.
- [11] Laure Bourgeois, Yong Zhang, Zehong Zhang, Yiqiang Chen, and Nikhil V Medhekar. 2020. Transforming solid-state precipitates via excess vacancies. *Nature communications* 11, 1 (2020), 1–10.
- [12] Bernard R Brooks, Charles L Brooks III, Alexander D Mackerell Jr, Lennart Nilsson, Robert J Petrella, Benoit Roux, Youngho Won, Georgios Archontis, Christian Bartels, Stefan Boresch, et al. 2009. CHARMM: the biomolecular simulation program. *Journal of computational chemistry* 30, 10 (2009), 1545–1614.
- [13] Roberto Car and Michele Parrinello. 1985. Unified approach for molecular dynamics and density-functional theory. *Physical Review Letters* 55, 22 (1985), 2471.
- [14] Paolo Carloni, Ursula Rothlisberger, and Michele Parrinello. 2002. The role and perspective of ab initio molecular dynamics in the study of biological systems. *Accounts of Chemical Research* 35, 6 (2002), 455–464.
- [15] Mohan Chen, Hsin-Yu Ko, Richard C. Remsing, Marcos F. Calegari Andrade, Biswajit Santra, Zhaoru Sun, Annabella Selloni, Roberto Car, Michael L. Klein, John P. Perdew, and Xifan Wu. 2017. Ab initio theory and modeling of water. *Proc. Natl. Acad. Sci. U.S.A.* 114 (Sept. 2017), 10846–10851.
- [16] Mohan Chen, Lixin Zheng, Biswajit Santra, Hsin-Yu Ko, Robert A DiStasio Jr, Michael L Klein, Roberto Car, and Xifan Wu. 2018. Hydroxide diffuses slower than hydronium in water because its solvated structure inhibits correlated proton transfer. *Nature chemistry* 10, 4 (2018), 413–419.
- [17] Wen-Kai Chen, Xiang-Yang Liu, Wei-Hai Fang, Pavlo O Dral, and Ganglong Cui. 2018. Deep Learning for Nonadiabatic Excited-State Dynamics. *The journal of physical chemistry letters* 9, 23 (2018), 6702–6708.
- [18] Stefan Chmiela, Alexandre Tkatchenko, Huziel E Sauceda, Igor Poltavsky, Kristof T Schütt, and Klaus-Robert Müller. 2017. Machine learning of accurate energy-conserving molecular force fields. *Science Advances* 3, 5 (2017), e1603015.
- [19] Andrew S. Clarke and Hannes Jónsson. 1993. Structural changes accompanying densification of random hard-sphere packings. *Phys. Rev. E* 47 (Jun 1993), 3975–3984. Issue 6. <https://doi.org/10.1103/PhysRevE.47.3975>
- [20] Fu-Zhi Dai, Bo Wen, Yinjie Sun, Huimin Xiang, and Yanchun Zhou. 2020. Theoretical prediction on thermal and mechanical properties of high entropy (Zr0.2Hf0.2Ti0.2Nb0.2Ta0.2)C by deep learning potential. *Journal of Materials Science & Technology* (2020).
- [21] Sambit Das, Phani Motamarri, Vikram Gavini, Bruno Turcksin, Ying Wai Li, and Brent Leback. 2019. Fast, scalable and accurate finite-element based ab initio calculations using mixed precision computing: 46 PFLOPS simulation of a metallic dislocation system. In *Proceedings of the International Conference for High Performance Computing, Networking, Storage and Analysis*. 1–11.
- [22] Robert A. DiStasio Jr, Biswajit Santra, Zhaofeng Li, Xifan Wu, and Roberto Car. 2014. The individual and collective effects of exact exchange and dispersion interactions on the ab initio structure of liquid water. *J. Chem. Phys.* 141 (Aug. 2014), 084502.
- [23] Markus Eisenbach, C-G Zhou, Don M Nicholson, Greg Brown, Jeff Larkin, and Thomas C Schulthess. 2009. A scalable method for ab initio computation of free energies in nanoscale systems. In *Proceedings of the Conference on High Performance Computing Networking, Storage and Analysis*. 1–8.
- [24] D. Frenkel and B. Smit. 2001. *Understanding molecular simulation*. Academic Press, Inc. Orlando, FL, USA.
- [25] Fei Gao and William J Weber. 2000. Atomic-scale simulation of 50 keV Si displacement cascades in β -SiC. *Physical Review B* 63, 5 (2000), 054101.
- [26] Francois Gygi, Erik W Draeger, Martin Schulz, Bronis R De Supinski, John A Gannels, Vernon Austel, James C Sexton, Franz Franchetti, Stefan Kral, Christoph W Ueberhuber, et al. 2006. Large-scale electronic structure calculations of high-Z metals on the BlueGene/L platform. In *Proceedings of the 2006 ACM/IEEE conference on Supercomputing*. 45–es.
- [27] Jiequn Han, Linfeng Zhang, Roberto Car, and Weinan E. 2018. Deep Potential: a general representation of a many-body potential energy surface. *Communications in Computational Physics* 23, 3 (2018), 629–639.
- [28] Yukihiko Hasegawa, Jun-Ichi Iwata, Miwako Tsuji, Daisuke Takahashi, Atsushi Oshiyama, Kazuo Minami, Taisuke Boku, Fumiyo Shoji, Atsuya Uno, Motoyoshi Kurokawa, et al. 2011. First-principles calculations of electron states of a silicon nanowire with 100,000 atoms on the K computer. In *Proceedings of 2011 International Conference for High Performance Computing, Networking, Storage and Analysis*. 1–11.
- [29] Bohumír Jelinek, Sébastien Groh, Mark F Horstemeyer, Jeffery Houze, Seong-Gon Kim, Gregory J Wagner, Amitava Moitra, and Michael I Baskes. 2012. Modified embedded atom method potential for Al, Si, Mg, Cu, and Fe alloys. *Physical Review B* 85, 24 (2012), 245102.
- [30] Hannes Jónsson and Hans C. Andersen. 1988. Icosahedral Ordering in the Lennard-Jones Liquid and Glass. *Phys. Rev. Lett.* 60 (May 1988), 2295–2298. Issue 22. <https://doi.org/10.1103/PhysRevLett.60.2295>
- [31] Ryan Jorn, Revati Kumar, Daniel P Abraham, and Gregory A Voth. 2013. Atomistic modeling of the electrode-electrolyte interface in Li-ion energy storage systems: electrolyte structuring. *The Journal of Physical Chemistry C* 117, 8 (2013), 3747–3761.
- [32] Alireza Khorshidi and Andrew A Peterson. 2016. Amp: A modular approach to machine learning in atomistic simulations. *Computer Physics Communications* 207 (2016), 310–324.
- [33] Hsin-Yu Ko, Linfeng Zhang, Biswajit Santra, Han Wang, Weinan E, Robert A DiStasio Jr, and Roberto Car. 2019. Isotope effects in liquid water via deep potential molecular dynamics. *Molecular Physics* 117, 22 (2019), 3269–3281.
- [34] Walter Kohn and Lu Jea Sham. 1965. Self-consistent equations including exchange and correlation effects. *Physical Review* 140, 4A (1965), A1133.
- [35] Kyuhyun Lee, Dongsun Yoo, Wonseok Jeong, and Seungwu Han. 2019. SIMPLENN: An efficient package for training and executing neural-network interatomic potentials. *Computer Physics Communications* 242 (2019), 95–103.
- [36] Kevin Leung and Susan B Rempe. 2005. Ab initio molecular dynamics study of glycine intramolecular proton transfer in water. *The Journal of chemical physics* 122, 18 (2005), 184506.
- [37] Xiaoxia Li, Zheng Mo, Jian Liu, and Li Guo. 2015. Revealing chemical reactions of coal pyrolysis with GPU-enabled ReaxFF molecular dynamics and cheminformatics analysis. *Molecular Simulation* 41, 1–3 (2015), 13–27.
- [38] Qianru Liu, Denghui Lu, and Mohan Chen. 2020. Structure and dynamics of warm dense aluminum: a molecular dynamics study with density functional theory and deep potential. *JOURNAL OF PHYSICS-CONDENSED MATTER* 32, 14 (APR 3 2020). <https://doi.org/10.1088/1361-648X/ab5890>
- [39] Alan C Lund, TG Nieh, and CA Schuh. 2004. Tension/compression strength asymmetry in a simulated nanocrystalline metal. *Physical Review B* 69, 1 (2004), 012101.
- [40] Chao Ma, Lei Wu, and Weinan E. 2019. Machine Learning from a Continuous Viewpoint. *arXiv preprint arXiv:1912.12777* (2019).
- [41] Aris Marcolongo, Tobias Binninger, Federico Zipoli, and Teodoro Laino. 2019. Simulating Diffusion Properties of Solid-State Electrolytes via a Neural Network Potential: Performance and Training Scheme. *ChemSystemsChem* (2019).
- [42] Dominik Marx and Jürg Hutter. 2009. *Ab initio molecular dynamics: basic theory and advanced methods*. Cambridge University Press.

[43] Aiichiro Nakano, Rajiv K Kalia, Ken-ichi Nomura, Ashish Sharma, Priya Vashishta, Fuyuki Shimojo, Adri CT van Duin, William A Goddard, Rupak Biswas, and Deepak Srivastava. 2007. A divide-and-conquer/cellular-decomposition framework for million-to-billion atom simulations of chemical reactions. *Computational Materials Science* 38, 4 (2007), 642–652.

[44] Ayako Nakata, Jack Baker, Shereif Mujahed, Jack TL Poulton, S Arapan, Jianbo Lin, Zamaan Raza, Sushma Yadav, Lionel Truflandier, Tsuyoshi Miyazaki, et al. 2020. Large scale and linear scaling DFT with the CONQUEST code. *arXiv preprint arXiv:2002.07704* (2020).

[45] S. Plimpton. 1995. Fast parallel algorithms for short-range molecular dynamics. *J. Comput. Phys.* 117, 1 (1995), 1–19.

[46] George D Purvis III and Rodney J Bartlett. 1982. A full coupled-cluster singles and doubles model: The inclusion of disconnected triples. *The Journal of Chemical Physics* 76, 4 (1982), 1910–1918.

[47] Jean-Yves Raty, Fran ois Gygi, and Giulia Galli. 2005. Growth of carbon nanotubes on metal nanoparticles: a microscopic mechanism from ab initio molecular dynamics simulations. *Physical review letters* 95, 9 (2005), 096103.

[48] Piotr T R o a ski and Micha  Zieli ski. 2016. Linear scaling approach for atomistic calculation of exciton properties of 10-million-atom nanostructures. *Physical Review B* 94, 4 (2016), 045440.

[49] J Schi tz, FD Di Tolla, and KW Jacobsen. 1998. Softening of nanocrystalline metals at very small grain sizes. *NATURE* 391, 6667 (FEB 5 1998), 561–563. <https://doi.org/10.1038/35328>

[50] J Schi tz and KW Jacobsen. 2003. A maximum in the strength of nanocrystalline copper. *SCIENCE* 301, 5638 (SEP 5 2003), 1357–1359. <https://doi.org/10.1126/science.1086636>

[51] Kristof Sch tt, Pieter-Jan Kindermans, Huziel Enoc Sauceda Felix, Stefan Chmiela, Alexandre Tkatchenko, and Klaus-Robert M ller. 2017. SchNet: A continuous-filter convolutional neural network for modeling quantum interactions. In *Advances in Neural Information Processing Systems*. 992–1002.

[52] Thomas P Senftle, Sungwook Hong, Md Mahbubul Islam, Sudhir B Kylasa, Yuanxia Zheng, Yun Kyung Shin, Chad Junkermeier, Roman Engel-Herbert, Michael J Janik, Hasan Metin Aktulga, et al. 2016. The ReaxFF reactive force-field: development, applications and future directions. *npj Computational Materials* 2, 1 (2016), 1–14.

[53] Andreas Singraber, J rg Behler, and Christoph Dellago. 2019. Library-Based LAMMPS Implementation of High-Dimensional Neural Network Potentials. *Journal of chemical theory and computation* 15, 3 (2019), 1827–1840.

[54] Justin S Smith, Olexandr Isayev, and Adrian E Roitberg. 2017. ANI-1: an extensible neural network potential with DFT accuracy at force field computational cost. *Chemical Science* 8, 4 (2017), 3192–3203.

[55] Grace M. Sommers, Marcos F. Calegari Andrade, Linfeng Zhang, Han Wang, and Roberto Car. 2020. Raman Spectrum and Polarizability of Liquid Water from Deep Neural Networks. *arXiv preprint arXiv:2004.07369* (2020).

[56] Mark Tuckerman. 2010. *Statistical mechanics: theory and molecular simulation*. Oxford university press.

[57] Priya Vashishta, Rajiv K Kalia, and Aiichiro Nakano. 1999. Large-Scale Atomistic Simulations of Dynamic Fracture. *Computing in science & engineering* 1, 5 (1999), 56–65.

[58] Priya Vashishta, Aiichiro Nakano, Rajiv K Kalia, and Ingvar Ebbsj . 1996. Crack propagation and fracture in ceramic films—million atom molecular dynamics simulations on parallel computers. *Materials Science and Engineering: B* 37, 1-3 (1996), 56–71.

[59] Hao Wang, Xun Guo, Linfeng Zhang, Han Wang, and Jianming Xue. 2019. Deep learning inter-atomic potential model for accurate irradiation damage simulations. *Applied Physics Letters* 114, 24 (2019), 244101.

[60] Han Wang, Linfeng Zhang, Jiequn Han, and Weinan E. 2018. DeePMD-kit: A deep learning package for many-body potential energy representation and molecular dynamics. *Computer Physics Communications* 228 (2018), 178–184.

[61] Junmei Wang, Romain M Wolf, James W Caldwell, Peter A Kollman, and David A Case. 2004. Development and testing of a general amber force field. *Journal of computational chemistry* 25, 9 (2004), 1157–1174.

[62] Lin-Wang Wang, Byounghak Lee, Hongzhang Shan, Zhengji Zhao, Juan Meza, Erich Strohmaier, and David H Bailey. 2008. Linearly scaling 3D fragment method for large-scale electronic structure calculations. In *SC'08: Proceedings of the 2008 ACM/IEEE Conference on Supercomputing*. IEEE, 1–10.

[63] Kun Yao, John E Herr, David W Toth, Ryker Mckintyre, and John Parkhill. 2018. The TensorMol-0.1 model chemistry: a neural network augmented with long-range physics. *Chemical science* 9, 8 (2018), 2261–2269.

[64] Jinzhe Zeng, Liguang Cao, Mingyuan Xu, Tong Zhu, and John ZH Zhang. 2019. Neural Network Based in Silico Simulation of Combustion Reactions. *arXiv preprint arXiv:1911.12252* (2019).

[65] Linfeng Zhang, Mohan Chen, Xifan Wu, Han Wang, , Weinan E, and Roberto Car. 2019. Deep neural network for the dielectric response of insulators. *arXiv preprint arXiv:1906.11434* (2019).

[66] Linfeng Zhang, Jiequn Han, Han Wang, Roberto Car, and Weinan E. 2018. Deep Potential Molecular Dynamics: A Scalable Model with the Accuracy of Quantum Mechanics. *Physical Review Letters* 120 (Apr 2018), 143001. Issue 14.

[67] Linfeng Zhang, Jiequn Han, Han Wang, Wissam Saidi, Roberto Car, and Weinan E. 2018. End-to-end Symmetry Preserving Inter-atomic Potential Energy Model for Finite and Extended Systems. In *Advances in Neural Information Processing Systems 31*, S. Bengio, H. Wallach, H. Larochelle, K. Grauman, N. Cesa-Bianchi, and R. Garnett (Eds.). Curran Associates, Inc., 4441–4451.

[68] Linfeng Zhang, De-Ye Lin, Han Wang, Roberto Car, and Weinan E. 2019. Active learning of uniformly accurate interatomic potentials for materials simulation. *Physical Review Materials* 3, 2 (2019), 023804.

[69] Yuzhi Zhang, Haidi Wang, Weijie Chen, Jinzhe Zeng, Linfeng Zhang, Han Wang, and Weinan E. 2020. DP-GEN: A concurrent learning platform for the generation of reliable deep learning based potential energy models. *Computer Physics Communications* (2020), 107206.